Elimination of threading dislocations in α-Ga_2O_3 by double-layered epitaxial lateral overgrowth

Katsuaki Kawara[1,2]*, Yuichi Oshima[3], Mitsuru Okigawa[1], and Takashi Shinohe[1]

[1]*FLOSFIA Inc., 1-29, Goryo ohara, Nishikyo-Ku, Kyoto 615-8245, Japan*

[2]*Graduate School of Engineering, Kyoto University, Katsura, Nishikyo-ku, Kyoto 615-8510, Japan*

[3]*National Institute for Materials Science, 1-1 Namiki, Tsukuba, Ibaraki 305-004, Japan*

E-mail: kawara@flosfia.com

Abstract

We demonstrated double-layered epitaxial lateral overgrowth (ELO) of α-Ga_2O_3 by halide vapor phase epitaxy. The second ELO α-Ga_2O_3 were regrown epitaxially and selectively through the windows of the patterned masks which were prepared on an ELO α-Ga_2O_3. The ELO islands coalesced step-by-step due to the nested-structure mask pattern. No dislocation was found by TEM not only above the masks but also above the windows of the second ELO pattern. The dislocation density was estimated to be less than 5×10^6 cm^{-2}. We obtained a continuous crystalline α-Ga_2O_3 film with a low density of dislocations in the entire second-ELO surface.

Corundum-structured alpha-gallium oxide (α-Ga_2O_3) is one of the most promising semiconductors for power device applications because of the large bandgap energy (E_g ~5.3 eV) and the expected high breakdown voltage.[1)] Indeed, Schottky barrier diodes composed of α-Ga_2O_3 films indicated high break down voltage of 531 V and low on-resistance of 0.1 mΩcm^2.[2)] α-Ga_2O_3 can make solid solutions with many other corundum-structured oxides such as sapphire with less compositional limitation compared to the case of β-Ga_2O_3. For example, it is possible to grow α-$(Al,Ga,In)_2O_3$ in a wide composition range, and the bandgap can be controlled between 3.8–8.8 eV.[3–8)] This advantage enables bandgap engineering with a large degree of freedom, which is essential to realize high-performance devices. Furthermore, it is possible to grow p-type corundum-structured α-Ir_2O_3 on α-Ga_2O_3 heteroepitaxially with an in-plane lattice mismatch of less than 0.3%[9)] to make a hetero pn junction, and α-Ga_2O_3-based normally-off MOSFET with a p-type well layer as an inversion layer has been demonstrated.[9–12)]

α-Ga_2O_3 is a high-pressure stable phase and thermodynamically meta-stable under ambient pressure.[13)] Therefore, it is difficult to grow bulk crystals of α-Ga_2O_3 by melt growth method, in contrast to the case of β-Ga_2O_3.[14–16)] Thus far, α-Ga_2O_3 films have been grown on foreign substrates with heteroepitaxial methods. Mist-CVD[1–3,11,12,17–20)] and halide vapor phase epitaxy (HVPE)[21–24)] on sapphire substrates have been mainly performed to obtain α-Ga_2O_3 films. One of the problems with the growth of α-Ga_2O_3 is the large lattice mismatch between α-Ga_2O_3 and sapphire (Δa/a ~4.5%, Δc/c ~3.3%).[25)] A high density of dislocations (~10^{10} cm^{-2}) which arise from the lattice mismatch propagate along the film growth direction in α-Ga_2O_3 films.[26)] Although the influence of the dislocations still remains to be studied in detail, the crystal quality of α-Ga_2O_3 films should be improved in order not to deteriorate the device performance.

Dislocation density in α-Ga_2O_3 films can be decreased by epitaxial lateral overgrowth (ELO).[25–29)] A typical ELO procedure is as follows. First, α-Ga_2O_3 thin (less than 3 μm) layer is grown on sapphire as a seed substrate. Second, periodic masks are formed on the template. Finally, α-Ga_2O_3 is regrown homoepitaxially through the mask windows. As a result, the quality of the regrown α-Ga_2O_3 can be improved by blocking and bending of dislocations. For example, Oshima *et al.* reported that the threading dislocation density in HVPE-grown ELO α-Ga_2O_3 was successfully decreased to be less than 5×10^6 cm^{-2}.[25)]

However, there still remained areas with a high density of dislocations above the ELO mask windows periodically,[25] and therefore the effect of reducing dislocations in α-Ga_2O_3 films was limited. The crystal quality of α-Ga_2O_3 films should be further improved to fabricate higher-voltage and lower-on-resistance power devices and to prevent the deterioration of the device performance. Thus, we developed double-layered ELO that can eliminate the threading dislocations remained on the window regions. The ELO process was performed twice so that the second ELO mask covered the first ELO windows to reduce the dislocation density in the entire surface of α-Ga_2O_3 films.

Figure 1(a) shows the schematic experimental process flow of the double-layered ELO of α-Ga_2O_3. The first ELO masks were prepared on a (0001) α-Ga_2O_3/sapphire template before the first ELO was performed by HVPE. The ELO α-Ga_2O_3 film was flattened by chemical mechanical polishing (CMP), and then the second ELO mask was formed on the flat surface. The second ELO was also performed by HVPE, and we obtained ELO α-Ga_2O_3 films. The double-layered ELO α-Ga_2O_3 films were observed with scanning electron microscopy (SEM) and transmission electron microscopy (TEM). Crystal structure of the ELO α-Ga_2O_3 was checked with selected area electron diffraction (SAED). The cross section of the ELO α-Ga_2O_3 films were processed for SEM by ion milling.

A home-build atmospheric horizontal hot-wall HVPE system was utilized for the growth. $GaCl_x$ and O_2 gasses were utilized as the precursors, and the source gases were transported by N_2 carrier gas with a dew point of below −90°C. $GaCl_x$ was generated upstream in the reactor by the reaction between high-purity metal Ga (6N grade) and HCl gas (5N grade) at 650°C. O_2 gas (6N5 grade) was supplied on the substrate downstream separately from $GaCl_x$. We grew α-Ga_2O_3 in the first ELO at 530°C with the HCl and O_2 partial pressures of 1.25×10^{-1} kPa and 1.25 kPa, respectively. The second ELO was performed at 510°C with two steps to fulfill both of growth rate and stability of crystal growth; first, the HCl and O_2 were supplied for 20 min with partial pressures of 1.25×10^{-1} kPa and 1.25 kPa, respectively, and then the partial pressures were increased without interruption to 5.00×10^{-1} kPa and 3.12 kPa, respectively.

Dot-patterned masks which possessed circle-shaped windows with a diameter of 5 μm were prepared by conventional photolithography. The windows of the first ELO mask were arranged to form a triangular lattice, and the distance between the edges of the nearest

windows was 20 μm (no figure). Ten-nm-thick sputtered TiO_2 was used as the mask material.

Figure 1(b) shows a plan-view and a cross-sectional schematic illustration of mask pattern for the second ELO mask. The second ELO windows were located on the laterally grown areas of the first ELO α-Ga_2O_3 island, where threading dislocations were blocked by the first ELO masks. The center areas of the first ELO α-Ga_2O_3 island, where threading dislocations propagated through the first ELO window, were covered by the second ELO masks. The diameter of the circle-shaped windows was 5 μm, and the distance between the edges of the nearest windows were 4 μm. Meanwhile, the distance between the edges of the nearest windows formed on the adjacent α-Ga_2O_3 areas was 10 μm. Such nested-structure mask pattern was employed so that α-Ga_2O_3 islands coalesce each other in a step-by-step manner, which would be effective to suppress the steep increase of tensile strain associated with the island coalescence.

The regrowth of α-Ga_2O_3 in the first ELO were stopped before complete coalescence. The isolated or incompletely coalesced α-Ga_2O_3 islands should be subjected to smaller strain compared to the case of complete coalescence, and therefore serious cracking or breakage of the substrate was avoided.

Figure 2 shows a cross-sectional SEM image of a film regrown on a first ELO layer with the second mask. The regrowth was performed with nominal thickness (i.e., the thickness for a flat film grown under the same growth conditions) of 10 μm. The bright contrast portions represent α-Ga_2O_3, and the dark contrast portions represent κ-Ga_2O_3 according to our previous study.[26] The second ELO masks were observed as horizontal lines on the first ELO layer flattened by CMP, and α-Ga_2O_3 islands were successfully regrown through the second ELO windows. At the same time, there were polycrystals on the second ELO masks. The lower half portion of the regrown islands in the regrowth layer in Fig. 2 were buried by the polycrystalline deposition.

Figure 3 shows an SAED pattern and a plan-view TEM image of an α-Ga_2O_3 island regrown in the second ELO step. We observed the incompletely coalesced island regrown above both windows and masks whose portions were able to be identified easily. It was confirmed that the crystal structure of the island was corundum. No dislocation was found not only above the second ELO mask but also directly above the second ELO window. Therefore, the threading dislocation density was estimated to be less than 5×10^6 cm^{-2} on

the basis that there was no dislocation in all area sampled as shown in Fig. 3. Thus, the periodically remained dislocations in the first ELO α-Ga_2O_3 were successfully eliminated and the crystalline quality of α-Ga_2O_3 islands was entirely improved by the double-layered ELO technique.

Figure 4(a)–(f) present the time evolution of the second ELO. Fig. 4(a), (b) show SEM images of homoepitaxially regrown α-Ga_2O_3 islands with a nominal thickness of 10 μm. The broken circle line represents the position of the first ELO window. Three α-Ga_2O_3 islands shown in Fig. 4(a) were regrown on single first ELO α-Ga_2O_3 area. The α-Ga_2O_3 islands were grown to over 5 μm (the size of the second ELO windows) in diameter. It was confirmed that α-Ga_2O_3 grew laterally above the second ELO masks. The lateral growth rate of α-Ga_2O_3 islands was larger than that of the polycrystalline κ-Ga_2O_3 deposition. Thus, the polycrystals on the second ELO masks should be buried by α-Ga_2O_3 islands with increasing growth time.

Figure 4(c), (d) show SEM images of the second ELO α-Ga_2O_3 with a nominal thickness of 73 μm. Islands grown on single first ELO α-Ga_2O_3 area coalesced into a larger island (hereafter called a cluster). The polycrystals deposited between the islands were buried as expected, whereas the polycrystals deposited between the clusters had not buried yet, and therefore the surface of the film was not completely covered with α-Ga_2O_3 at this stage. The α-Ga_2O_3 clusters were grown to a height of over 20 μm. Meanwhile, the α-Ga_2O_3 clusters had not coalesced with each other yet due to the intentional large spacing of windows.

Figure 4(e), (f) show SEM images of the second ELO α-Ga_2O_3 with a nominal thickness of 86 μm. The α-Ga_2O_3 clusters were coalesced with each other and the polycrystals between the clusters were buried. The step-by-step coalescence of α-Ga_2O_3 in the second ELO was successfully achieved. The shape of α-Ga_2O_3 islands and clusters became irregular in comparison with that of the first ELO α-Ga_2O_3 islands partly because the surface cleaning and the film-surface flatness after CMP was insufficient for symmetrical regrowth of α-Ga_2O_3.

The second ELO mask design made the difference between the distance among the islands and that of the clusters, leading to the step-by-step coalescence in the second ELO of α-Ga_2O_3. The rapid increase of the tensile strains caused by the simultaneous coalescence of islands was avoided. Considering the model Nix *et al*. proposed,[30] the tensile stress in the

second ELO α-Ga_2O_3 was reduced sufficiently to prevent serious cracking or breakage of the substrate because the α-Ga_2O_3 islands possessed fewer side surfaces concerned with coalescence in comparison with conventional ELO. In fact, the second ELO film had no serious cracking despite the fact the film thickness was as large as ~75 μm.

Figure 5 shows SEM images of the same sample as shown in Fig. 4(e), (f) taken with low magnification. The first ELO layer and the polycrystalline depositions on the second ELO masks were completely covered with an α-Ga_2O_3 layer regrown in the second ELO, although the surface was still bumpy. The film thickness was ~100 μm, and the α-Ga_2O_3 layer in the second ELO layer was more than 20 μm in thickness. A continuous α-Ga_2O_3 film with high quality was obtained with the double-layered ELO.

In summary, we demonstrated the double-layered ELO of α-Ga_2O_3 by HVPE. The patterned masks with nested structure were prepared on the first ELO α-Ga_2O_3, and α-Ga_2O_3 islands were epitaxially regrown through the mask windows. The second ELO α-Ga_2O_3 islands grew selectively and coalesced each other in a step-by-step manner owing to the nested-structure mask pattern. No dislocation was observed by TEM not only above the masks but also above the windows of second ELO. The dislocation density was estimated to be less than 5×10^6 cm^{-2}. We obtained a continuous crystalline α-Ga_2O_3 film with a low density of dislocations in the entire second-ELO surface.

Acknowledgments

Part of this work was supported by the New Energy and Industrial Technology Development Organization (NEDO).

References

1) D. Shinohara and S. Fujita, Jpn. J. Appl. Phys. **47**, 7311 (2008).
2) M. Oda, R. Tokuda, H. Kambara, T. Tanikawa, T. Sasaki, and Toshimi Hitora, Appl. Phys. Express **9**, 021101 (2016).
3) S. Fujita and K. Kaneko, J. Cryst. Growth **401**, 588 (2014).
4) F. Zhang, K. Saito, T. Tanaka, M. Nishio, M. Arita, and Q. Guo, Appl. Phys. Lett. **105**, 162107 (2014).
5) H. Ito, K. Kaneko, and S. Fujita, Jpn. J. Appl. Phys. **51**, 100207 (2012).
6) K. Kaneko, K. Suzuki, Y. Ito, and S. Fujita, J. Cryst. Growth **436**, 150 (2016).
7) F. Zhang, K. Saito, T. Tanaka, M. Nishio, M. Arita, and Q. Guo, Solid State Commun, **186**, 28 (2014).
8) T. Wang, W. Li, C. Ni, and A. Janotti, Phys. Rev. Appl. **10**, 011003 (2018).
9) S. Kan, S. Takemoto, K. Kaneko, I. Takahashi, M. Sugimoto, T. Shinohe, and S. Fujita, Appl. Phys. Lett. **113**, 212104 (2018).
10) S. Kan, S. Takemoto, K. Kaneko, T. Shinohe, and S. Fujita, IEEE CPMT Symposium Japan, Kyoto, 2018, pp. 95–98.
11) K. Kaneko, S. Fujita, and T. Hitora, Jpn. J. Appl. Phys. **57**, 02CB18 (2018).
12) FLOSFIA and Kyoto univ: News release, July 13 (2008). http://flosfia.com/20180713/
13) D. Machon, P. F. McMillan, B. Xu, and J. Dong, Phys. Rev. B **73**, 094125, (2006).
14) E. G. Víllora, K. Shimamura, Y. Yoshikawa, K. Aoki, and N. Ichinose, J. Cryst. Growth **270**, 420 (2004).
15) H. Aida, K. Nishiguchi, H. Takeda, N. Aota, K. Sunakawa, and Y. Yaguchi, Jpn. J. Appl. Phys. **47**, 8506 (2008).
16) Z. Galazka, K. Irmscher, R. Uecker, R. Bertram, M. Pietsch, A. Kwasniewski, M. Naumann, T. Schulz, R. Schewski, D. Klimm, and M. Bickermann, J. Cryst. Growth **404**, 184 (2014).
17) T. Kawaharamura, G. T. Dang, and M. Furuta, Jpn. J. Appl. Phys. **51**, 040207 (2012).
18) M. Oda, K. Kaneko, S. Fujita, and Toshimi Hitora, Jpn. J. Appl. Phys. **55**, 1202B4 (2016).
19) H. Nishinaka, D. Tahara, S. Morimoto, and M. Yoshimoto, Mater. Lett. **205**, 28 (2017).
20) Y. Cheng, Y. Xu, Z. Li, J. Zhang, D. Chen, Q. Feng, S. Xu, H. Zhou, J. Zhang, Y. Hao, and C. Zhang, J. Alloys Compd. **831**, 154776 (2020).

21) Y. Oshima, E. G. Villora, and K. Shimamura, Appl. Phys. Express **8**, 055501 (2015).
22) Y. Oshima, K. Kawara, T. Oshima, M. Okigawa, and T. Shinohe, Semicond Sci Technol **35**, 055022 (2020).
23) A. I. Pechnikov, S. I. Stepanov, A. V. Chikiryaka, M. P. Scheglov, M. A. Odnobludov, and V. I. Nikolaev, Semiconductors **53**, 780 (2019).
24) H. Son and D. W. Jeon, J. Alloys Compd. **773**, 631 (2019).
25) Y. Oshima, K. Kawara, T. Shinohe, T. Hitora, M. Kasu, and S. Fujita, APL Mater. **7**, 022503 (2019).
26) Y. Oshima, K. Kawara, T. Oshima, M. Okigawa, T. Shinohe, Jpn. J. Appl. Phys. **59**, 025512 (2020).
27) H. Son, Y. J. Choi, J. S. Ha, S. H. Jung, and D. W. Jeon, Cryst. Growth Des. **19**, 5105 (2019).
28) A. N. Cha, S. Bang, H. Rho, H. Bae, D. W. Jeon, J. W. Ju, S. K. Hong, and J. S. Ha, Appl. Phys. Lett. **115**, 091605 (2019).
29) R. Jinno, N. Yoshimura, K. Kaneko, and S. Fujita, Jpn. J. Appl. Phys. **58**, 120912 (2019).
30) W. D. Nix and B. M. Clemens, J. Mater. Res. **14**, 3467 (1999).

Figure Captions

Fig. 1. Schematic process flow of (a) double-layered ELO of α-Ga_2O_3 and (b) mask pattern for second ELO of α-Ga_2O_3.

Fig. 2. Cross-sectional SEM image of a film regrown on a template for second ELO of α-Ga_2O_3.

Fig. 3. (a) Plan-view SEM image of the island which was observed by TEM. (b) Plan-view TEM image of a second ELO α-Ga_2O_3 island. The area surrounded by broken line was above the second ELO mask and the other area was above the second ELO window. (c), (d) SAED patterns of the island. The SAED images were observed at the circled areas in (b).

Fig. 4. Plan-view and cross-sectional SEM images of second ELO of α-Ga_2O_3 with nominal thickness (i.e., thickness for the flat films) of (a), (b) 10 μm, (c), (d) 73 μm, (e), (f) 87 μm.

Fig. 5. (a) Plan-view and (b) cross-section SEM images of second ELO of α-Ga_2O_3. Note that the top layer of the film was composed of only α-Ga_2O_3.

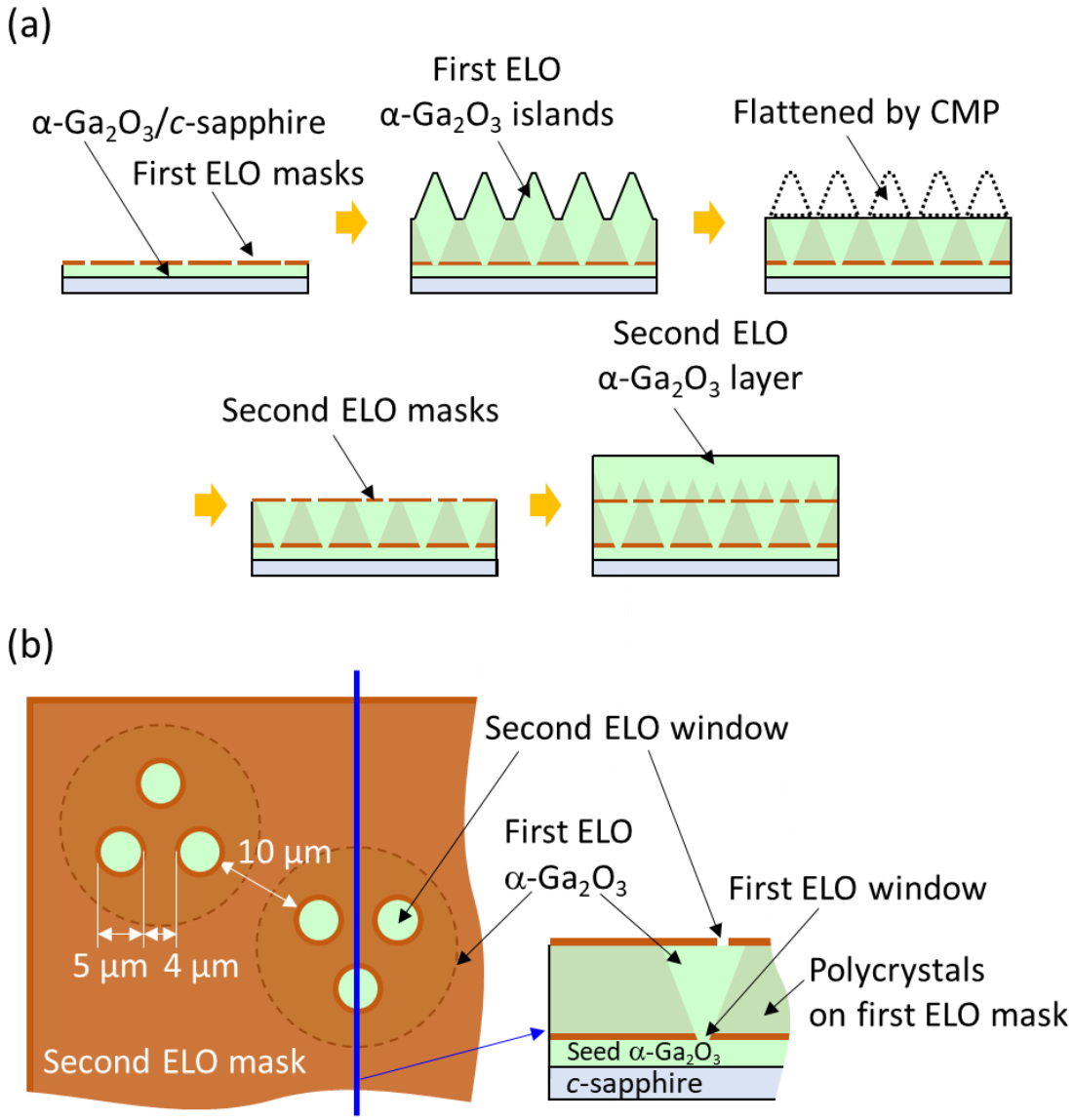
(a)
α-Ga2O3/c-sapphire
First ELO masks
First ELO
α-Ga2O3 islands
Flattened by CMP
Second ELO masks
Second ELO
α-Ga2O3 layer
(b)
10 μm
5 μm
4 μm
Second ELO mask
Second ELO window
First ELO
α-Ga2O3
First ELO window
Polycrystals
on first ELO mask
Seed α-Ga2O3
c-sapphire

Fig.1.

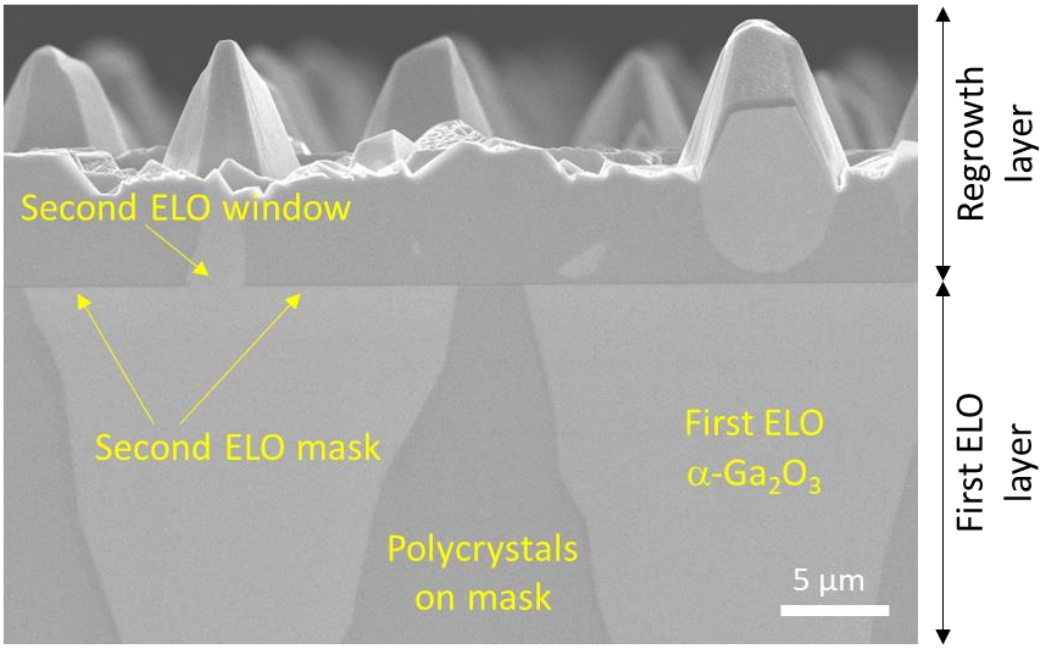
Second ELO window
Second ELO mask
First ELO
α-Ga2O3
Polycrystals
on mask
5 μm
Regrowth
layer
First ELO
layer

Fig. 2.

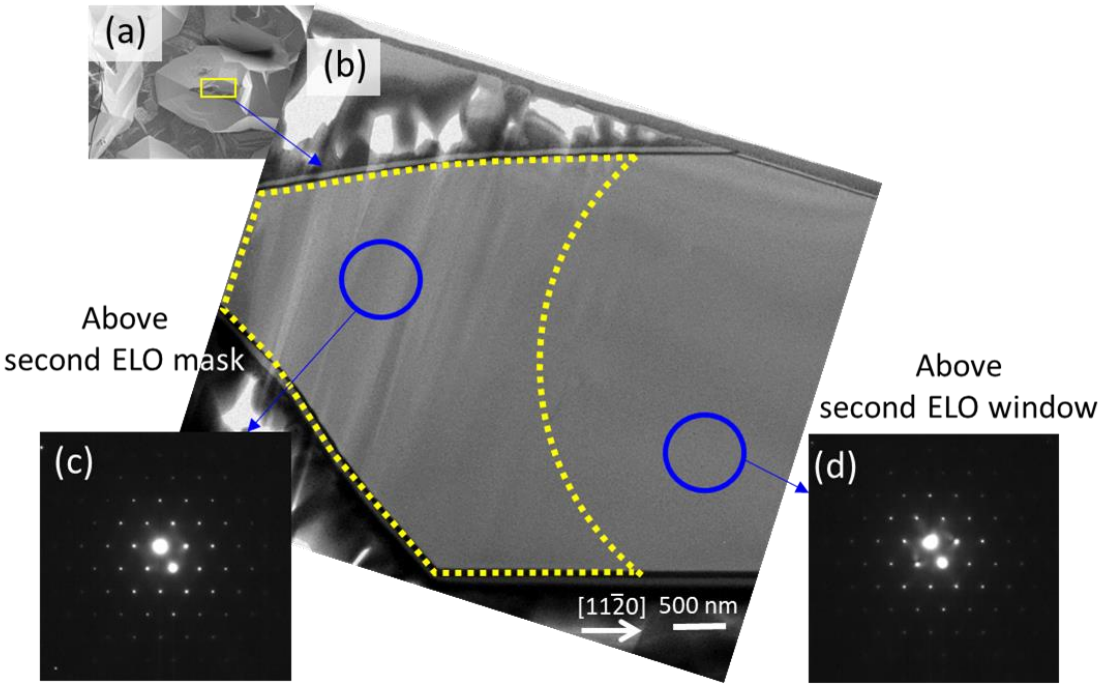
(a)
(b)
Above
second ELO mask
Above
second ELO window
(c)
(d)
[11$\bar{2}$0] 500 nm

Fig. 3.

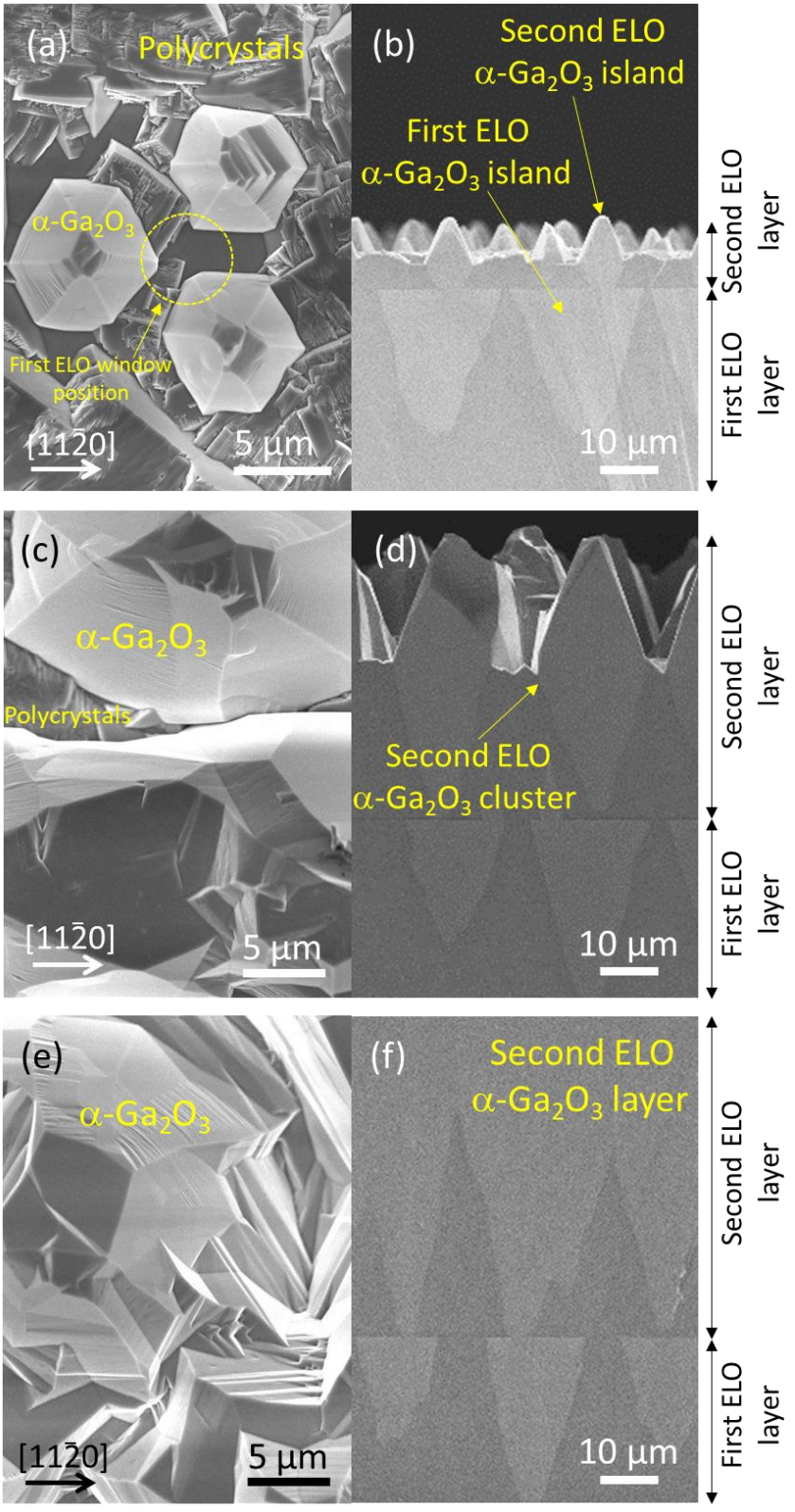
(a)
Polycrystals
α-Ga2O3
First ELO window position
[11$\bar{2}$0]
5 μm
(b)
Second ELO α-Ga2O3 island
First ELO α-Ga2O3 island
10 μm
Second ELO layer
First ELO layer
(c)
α-Ga2O3
Polycrystals
[11$\bar{2}$0]
5 μm
(d)
Second ELO α-Ga2O3 cluster
10 μm
Second ELO layer
First ELO layer
(e)
α-Ga2O3
[11$\bar{2}$0]
5 μm
(f)
Second ELO α-Ga2O3 layer
10 μm
Second ELO layer
First ELO layer

Fig. 4.

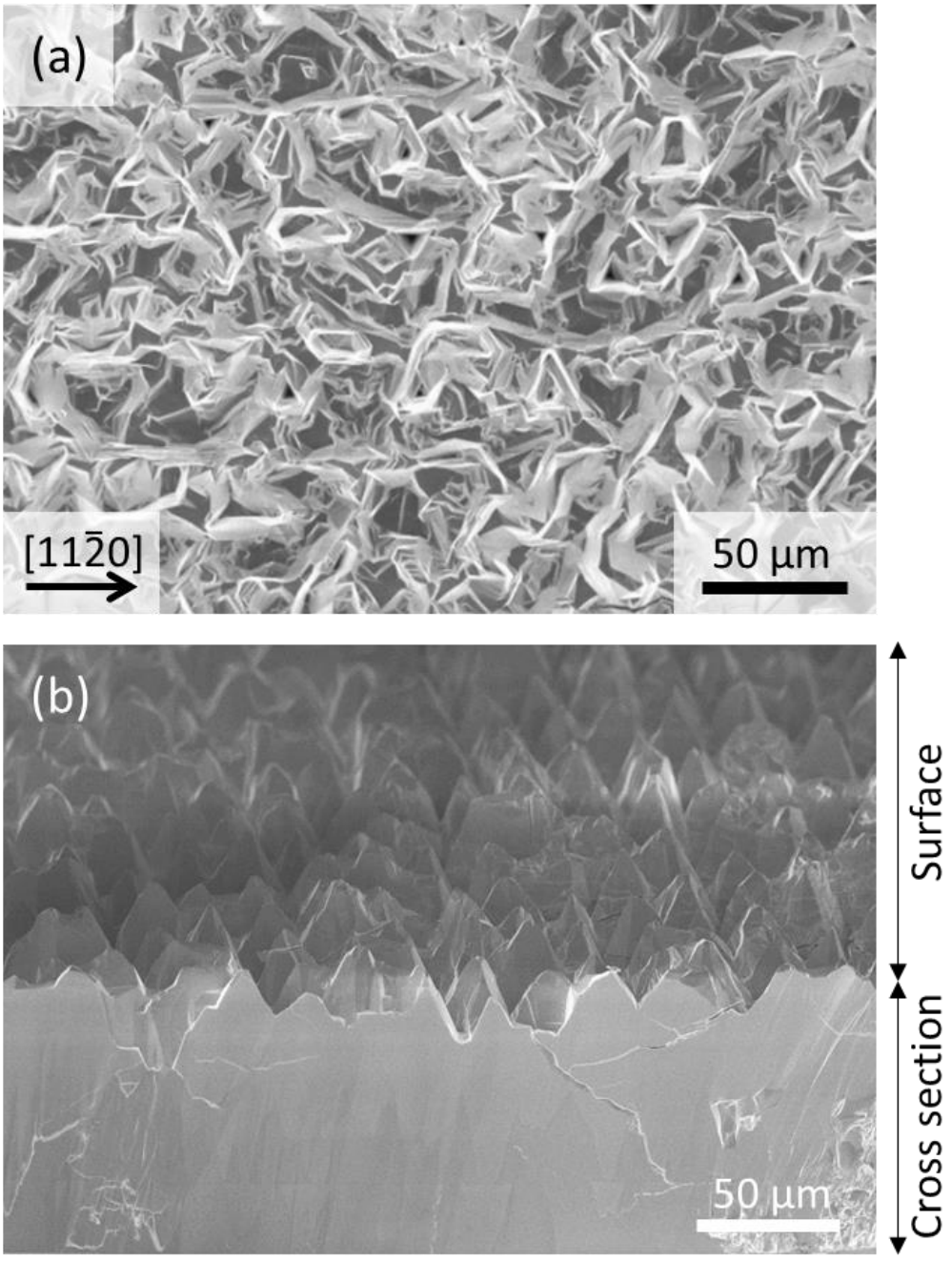

Fig. 5